PAPER • **OPEN ACCESS**

Process-related influences and correlations in wire arc additive manufacturing of high-strength steels

To cite this article: D Schroepfer *et al* 2021 *IOP Conf. Ser.: Mater. Sci. Eng.* **1147** 012002

Process-related influences and correlations in wire arc additive manufacturing of high-strength steels

D Schroepfer[1,*], R Scharf-Wildenhain[2], A Haelsig[2], K Wandtke[1], A Kromm[1] and T Kannengiesser[1]

[1] Bundesanstalt für Materialforschung und -prüfung (BAM)
[2] Technische Universität Chemnitz, Professur Schweißtechnik

[*]e-mail: dirk.schroepfer@bam.de

Abstract. High-strength fine-grained structural steels have great potential for weight-optimized, efficient structures in many modern steel applications. Further advances in efficiency can be achieved through additive manufacturing and bionic design. Commercial high-strength filler materials for wire arc additive manufacturing (WAAM) are already provided by the consumable producers. Today, application would be strictly limited due to absence of quantitative findings or any guidelines for the industry regarding welding-related stresses and component safety during manufacturing and service. Hence, process- and material-related influences and design-related restraint conditions associated with formation of residual stresses and cold cracking risk are investigated. The aim is the accessibility of special WAAM self-restraining cold cracking tests and easy applicable processing recommendations, enabling an economical, fit-for-purpose and crack-safe WAAM of high-strength steels. This first study focuses on determination of interactions between WAAM process parameters, resulting layer geometry, microstructure and residual stresses, analyzed via X-ray diffraction. Defined reference specimens are automated welded using a special WAAM solid wire (yield strength >820 MPa). Geometric properties can be specifically adjusted by wire feed and welding speed, but cannot be varied arbitrarily, since a high heat input causes local overheating, inadmissible changes of microstructure and mechanical properties, defects and comparable high tensile residual stresses.

1. Introduction

Due to economic and design aspects, high-strength fine-grained structural steels are nowadays increasingly applied in modern steel structures, e.g. in building construction, plant engineering and crane construction. By utilizing fine-grain structural steels with higher yield strengths (≥690 MPa), considerable weight reductions and lower processing costs can be achieved by reducing wall thickness. For example, by substituting S960QL for S235J2, the weight can be reduced by up to 78% [1, 2]. Current efforts towards lightweight construction result from the goal of reducing greenhouse gas emissions by up to 62% by 2030 compared to 1990. These requirements mean that process emissions in industry must be reduced by increasing energy, raw material and material efficiency [3]. This often leads to more complex components and structures. Today, additive manufacturing for the modification or production of high-strength components offers many economic advantages over conventional processes and a significant gain in design freedom, for example, to create bionic designs [4]. In addition, near-net-shape components can often save costly machining steps [5]. In particular, the use of high-strength fine-grain structural steels has great potential for weight-optimized, efficient

structures with high mechanical strength for many areas of steel construction. In conventional production, the most important welding process is gas metal arc welding (GMAW). Based on GMAW, the shape-giving process wire arc additive manufacturing (WAAM) has been developed in recent years. Furthermore, special welding wires for the production of high-strength components using WAAM, developed on the base of high-strength filler materials for joint welding, are already available on the market [6].

WAAM is particularly suitable for generating complex structures due to its high deposition rates, process reliability and good automatability [4, 5]. The basic applicability for large-format components using welding robots has already been proven in several studies [4, 7]. Depending on the dimensions of the component, commercially available welding consumables as well as finished WAAM welding systems in various sizes are now available, with which components can be generated by multi-axis portals or robots [8]. Modified GMAW short arc processes are particularly suitable for large-volume components (e.g. Cold Metal Transfer, CMT) due to their high deposition rate at low heat input [9]. In welding experiments and accompanying numerical simulations, the high dependence of the temperature distribution and the resulting component geometry on the production parameters could be demonstrated [10, 11]. These studies confirmed that adequate heat conduction in the WAAM process represents a major challenge for the special microstructure of high-strength fine-grained structural steels. The necessary cooling rates to achieve the required microstructure and mechanical properties (e.g. $t_{8/5}$ time for S690: approx. 5 s to 20 s) can only be achieved by limiting the component temperatures and heat input. For this purpose, build-up strategy and heat control (energy per unit length and preheating or interpass temperature) must be adapted in such a way that as little heat as possible is introduced during production [12]. With regard to the heat control of fine-grained structural steels, there are processing guidelines (e.g. EN1011-2, SEW088 [13, 14]) based on carbon equivalents, such as the CET. However, these are mainly based on tests on steels with lower strength. In addition, in guidelines for the design of structures, residual stresses are generally assumed to be equal to the yield strength in the weld [15].

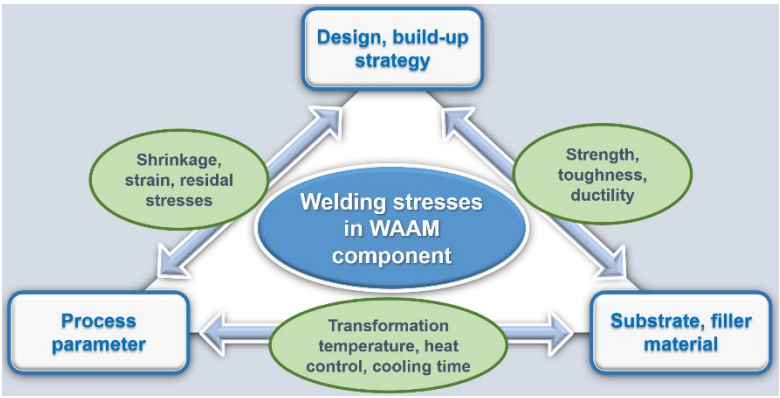

Figure 1. Complex interaction of influences on residual stresses in WAAM components.

Hence, there is still a lack of quantitative information on the production-related stresses and component safety during manufacture and operation that would prevent extensive industrial application [12, 16]. Moreover, many applications require high dimensional accuracy and component integrity due to safety, cost and technological aspects. For the production of high-strength components, generative and machining production steps can be used in a complementary manner. For this purpose, however, as shown in figure 1 comprehensive knowledge of the complex interactions between the welding process and heat conduction during production, the metallurgical processes and the existing design influences on the residual stresses arise is necessary [17, 18]. Thus, in order to reliably avoid high welding-related residual stress levels and possible resulting crack formations during production or a pre-mature component failure, recommendations regarding welding process, heat control, build-up strategy, design and material selection are necessary [12, 19]. Furthermore, the

effects of separating processes by removing the substrate plate or by machining the preforms should be clarified, since these affect the residual stress state and may cause significant distortion of the components [20].

In this regard, systematic investigations are currently being carried out in a research project of TU Chemnitz and BAM (FOSTA P1380/IGF 21162 BG). The present work deals with the basic relationships between the welding parameters, the resulting cooling time and the generated layer geometry. Furthermore, the resulting residual stresses are quantified and compared regarding the application of different welding or heat input values, respectively.

2. Experimental and materials

2.1. WAAM processing system

The configuration of the robot-supported WAAM system at TU Chemnitz consists of a 6 axis-robot system (KR 6 by KUKA) and a welding machine (TransPuls Synergic, TPS 5000, by Fronius). The robot controller, the central processing unit of the robot system, interprets the robot program codes and moves the manipulator along the programmed paths. A programmable logic controller (PLC) communicates with the external system components. Figure 2 shows the block diagram of the complete welding system. A robot interface serves as a link between the robot controller and the welding system. The commands for the welding system and motion of the robot are located in the corresponding program line of the robot program, which are interpreted and send by the controller to the robot (movement) and the welding system (welding commands). Besides the welding speed due to traveling speed of the robot, the modified short arc welding process CMT, used for these investigations, is adjusted due to the parameters wire feed speed, arc correction and dynamics. The used programming language for the robot system interface enables the integration of several functions allowing special commands for different movement modes or for the control of external systems components. The program is basically extracted and compiled from a CAD model via a slicer, which generates a tool path for the motion planning. This process is also parametric and real-time capable to react on differences or changes to the CAD geometry. These procedures were developed at TU Chemnitz.

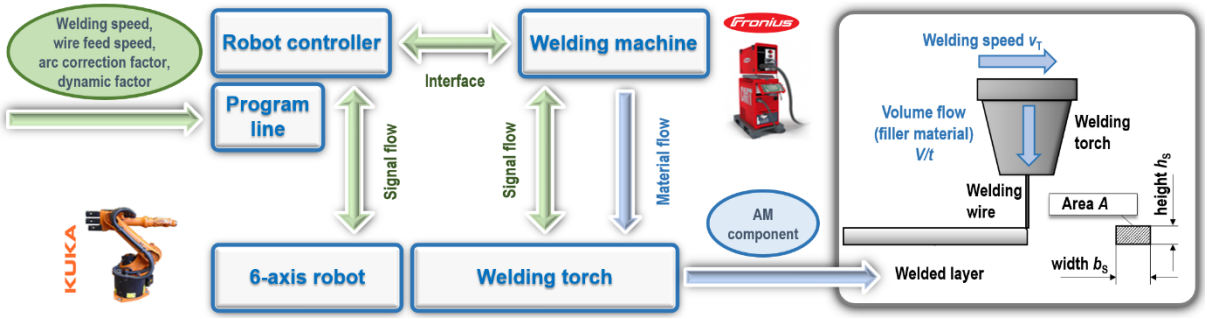

Figure 2. Signal and material flow of the robot-supported WAAM welding system; welding parameters (welding speed v_T, volume flow per time V/t) determining layer width b_S and height h_S.

2.2. Materials

In the study, a special for WAAM developed high-strength filler material 10NiMnMoCr8-7-6 (3Dprint AM 80 HD, abbreviation: AM 80, by voestalpine Böhler Welding Germany) having a diameter of 1.2 mm is used. Compared to conventional high-strength solid wire consumables of similar yield strength with a minimum of 790 MPa, e.g. G 79 5 M21 Mn4Ni1.5CrMo (EN ISO 16834-A), the modification of the composition for WAAM welding allows optimised deposition conditions for layer-by-layer build-up. Furthermore, an increase in the manufacturing degrees of freedom is achievable and, with regard to welding heat control, extended processing windows, which still ensure the required

mechanical properties. Table 1 shows the chemical composition and mechanical properties of the investigated welding filler material. The substrate was a 4 mm thick plate of high-strength steel S690QL with a minimum yield strength of 690 MPa. According to the steel producers' recommendations this allows welding in a similar working range regarding heat control for both substrate and filler material to ensure a proper fusion of the component to the substrate. In addition, due to the lower strength a rather higher ductility and thus moderate rigidity conditions are obtained when welding the components.

Table 1. Chemical composition (in wt.-%, Fe balanced) and mechanical properties of filler material 3Dprint AM 80 HD according to the producer (Böhler) in the recommended $t_{8/5}$ range of 5 s to 20 s [6].

C	Si	Mn	Cr	Mo	Ni	$R_{p0.2}$	R_m	A_5
0.09	0.40	1.70	0.35	0.60	2.00	820 MPa	920 MPa	20%

2.3. Welding experiments

During additive manufacturing, the robot moves the welding torch at a constant speed along a programmed path. The welding system presented in figure 2 feeds the filler wire with a defined wire feeding speed or volume flow, respectively. Assuming a rectangular layer cross-section, equation (1) describes the relationship between the layer width b_S, height h_S and the cross-section A:

$$A = b_S \cdot h_S = \frac{V}{t} \cdot \frac{1}{v_T} \tag{1}$$

Consequently, both wire feed and welding speed have an influence on the cross-section of the applied weld bead [4]. Furthermore, these parameters are the main influencing factors of the energy per unit length and thus also determine the flow and solidification behavior of the metallic melt by the amount of heat applied. In order to meet the requirements on geometric specifications, a systematic knowledge of these correlations in the desired parameter range is required. Hence, the focus of this study is on the systematic investigation of these welding parameters and their influence on the layer geometry. For this purpose, component geometries were manufactured as open hollow cuboids by applying 11 layer-wise seams, as shown in figure 3a. The $t_{8/5}$ cooling time was determined during the process by means of a thermocouple (type K) in the 5th layer. The process parameters for these experimental test series are shown in table 2.

Table 2. Constant welding parameters for the experiments.

Welding machine (TPS 5000) characteristic	Arc correc-tion factor	Dynamic factor	Preheating temperature	Interpass temperature	Shielding gas
C1622	–15%	4	20 °C	200 °C	98% Ar, 2% CO_2

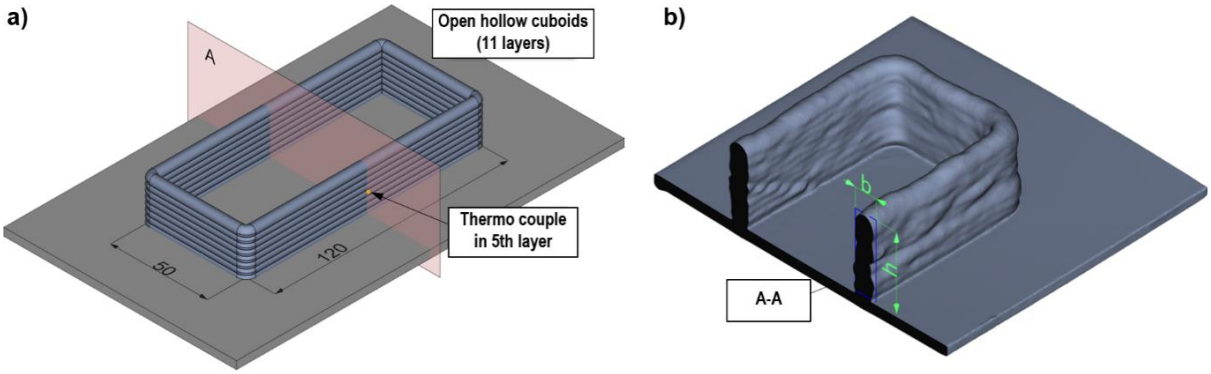

Figure 3. a) Open hollow cuboid with 11 layers, thermo couple type K (determination of $t_{8/5}$ cooling time); b) non-destructive evaluation of test specimens using 3D scan: determination of web height and width in cross section A-A using bounding box.

By systematically varying the parameters of the welding and wire feed speed, a total of 16 open hollow cuboids were produced (V1 to V16). The test matrix is presented in table 3. To evaluate these tests, a 3D scan of the components was performed (accuracy: ±0.05 mm). The side walls of the open hollow cuboids were analyzed with regard to web height and width in the symmetry planes of the test samples. Figure 3b shows this exemplary for one side by means of a digitized sample geometry in cross section A-A. For each hollow cuboid, web heights and widths were measured at four defined positions. The averaged layer dimensions height h_S and width b_S can be calculated using equations (2) and (3) with web height h_i, web width b_i and amount of layer n:

$$h_S = \frac{1}{4 \cdot n} \sum_{i=1}^{4} h_i \tag{2}$$

$$b_S = \frac{1}{4} \sum_{i=1}^{4} b_i \tag{3}$$

Table 3. Test matrix for determining the layer geometry dependent on welding and wire feed speed (bold test numbers: residual stress analysis performed).

		Welding speed [cm/min]			
		20	30	40	50
Wire feeding speed [m/min]	2	V1	V5	**V9**	V13
	3	V2	V6	V10	V14
	4	V3	**V7**	V11	V15
	5	V4	V8	V12	V16

2.4. Residual stress analysis

X-ray diffraction (XRD) was used to analyze the local residual stresses transverse and longitudinal to the weld via the $\sin^2\Psi$-method. This was performed at several positions on the top layer of the hollow cuboid specimens to determine the effect of the heat input due to varied wire feeding and welding speed. The measuring lines are shown in figure 4. Two test specimens were analyzed from the test matrix: V7 (heat input E=0.43 kJ/mm, $t_{8/5}$=20.2 s) and V9 (E=0.18 kJ/mm, $t_{8/5}$=9.2 s) to observe the effect in lower and upper scope regarding the recommended $t_{8/5}$ cooling time range of $t_{8/5}$. Table 4 shows the used parameters for the residual stress analysis.

Table 4. Parameters for residual stress analysis by means of XRD ($\sin^2\Psi$-method).

Radiation:	Tupe power:	Collimator:	Detector:
CrKα	30 kV/6.7 mA	2 mm	Linear solid state detector
Diffraction line:	Ψ-tilting:	Ψ-steps:	Measuring time:
{211}α	0° to ±45°	9	5 s

3. Results and discussion

3.1. Microstructure

Figure 5 shows a microsection of the weld metal of a generated wall after production with a constant interlayer temperature of 200 °C and a $t_{8/5}$ cooling time of approx. 10 s. The cross section shows a suitable, fine-grained microstructure. Compared to conventional filler materials, e.g. G 79, the especially for WAAM developed welding wire (AM 80) tends to solidify more fine-grained at similar welding parameters in the recommended $t_{8/5}$ cooling time range of 5 s to 20 s.

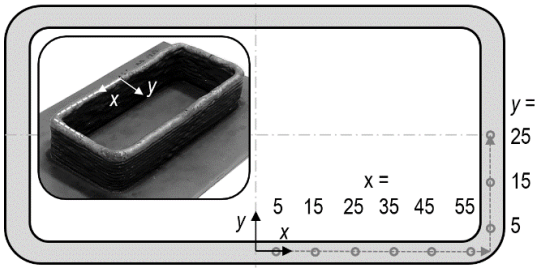

Figure 4. Measuring lines for residual stress analyses at the test specimen.

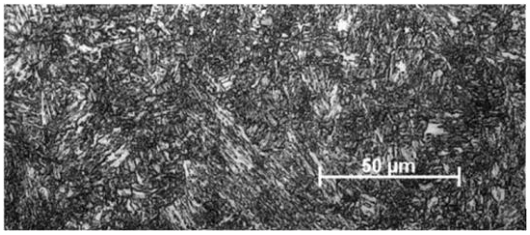

Figure 5. Cross section of the weld metal (AM 80) for $t_{8/5}$ cooling time of approx. 10 s.

3.2. Layer and component dimension

Table 5 summarizes the averaged layer widths b_s and heights h_s as a function of the welding and wire feed speed. Based on these measurement data for the component or layer geometry, the characteristics of the WAAM production in the investigated parameter range can be modelled. Figure 6 shows the contour plot of the average layer dimensions (width (a); height (b)) as a function of wire feeding v_W and welding speed v_T for the derived regression model. In the regression model v_W and v_T are highly significant. Also, the squared interaction of v_T is significant for both b_S and h_S with a p value of 0.04 and 0.01 respectively. The model qualities are high with R^2=0.988 and R^2=0.996, respectively.

Table 5. Results for averaged layer geometry (b_s, h_s), heat input E and resulting cooling time $t_{8/5}$ dependent on welding speed v_T and wire feed speed v_W.

			Welding speed v_T [cm/min]			
		Results	20	30	40	50
Wire feeding speed v_W [m/min]	2	b_s [mm] / h_s [mm]	5.4 / 2.2	4.6 / 2.0	**3.9 / 1.8**	3.4 / 1.6
		E [kJ/mm] / $t_{8/5}$ [s]	0.36 / 12.6	0.24 / 10.4	**0.18 / 9.2**	0.14 / 5.8
	3	b_s [mm] / h_s [mm]	6.9 / 2.5	5.6 / 2.2	4.9 / 2.0	4.5 / 1.8
		E [kJ/mm] / $t_{8/5}$ [s]	0.51 / 19.4	0.34 / 14.0	0.25 / 11.8	0.20 / 9.1
	4	b_s [mm] / h_s [mm]	7.8 / 2.7	**6.7 / 2.4**	5.8 / 2.2	5.3 / 2.0
		E [kJ/mm] / $t_{8/5}$ [s]	0.65 / 25.6	**0.43 / 20.2**	0.32 / 14.2	0.26 / 13.0
	5	b_s [mm] / h_s [mm]	8.8 / 2.9	7.7 / 2.6	7.4 / 2.4	6.2 / 2.2
		E [kJ/mm] / $t_{8/5}$ [s]	0.79 / 40.0	0.53 / 26.4	0.40 / 18.2	0.32 / 13.8

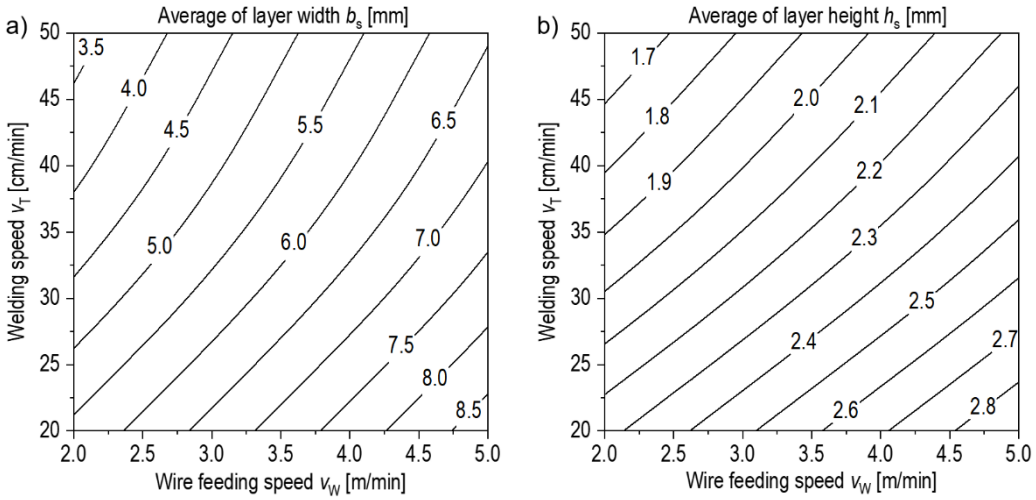

Figure 6. Average layer width (a) and height (b) as a function of wire feeding and welding speed in the investigated parameter range (contour plots of the regression models).

The layer width almost linearly increases with higher values for wire feeding speed and lower values for welding speed. For the layer height the same trend can be observed. Comparing both, it reveals that for higher values the influence of welding speed on the layer width decreases and then depends to a greater extent on the wire feeding speed, in contrast to the effect on the layer height. This finally also exhibits that the width and height of the generated layers depend largely on the energy per unit length used. In this context, figure 7a shows the contour diagram of energy per unit length as a function of wire feed rate and welding speed. The derived regression model for heat input shows highly significant effects for the wire feed rate, welding speed, their interaction, and a highly significant quadratic effect of welding speed with a model quality of R^2=0.995. Compared to figure 6, as expected, increased layer heights and widths correlate with a higher heat input, so that an almost linear relationship exists. In addition, the cooling time $t_{8/5}$ correlates with these results which is presented in figure 7b.

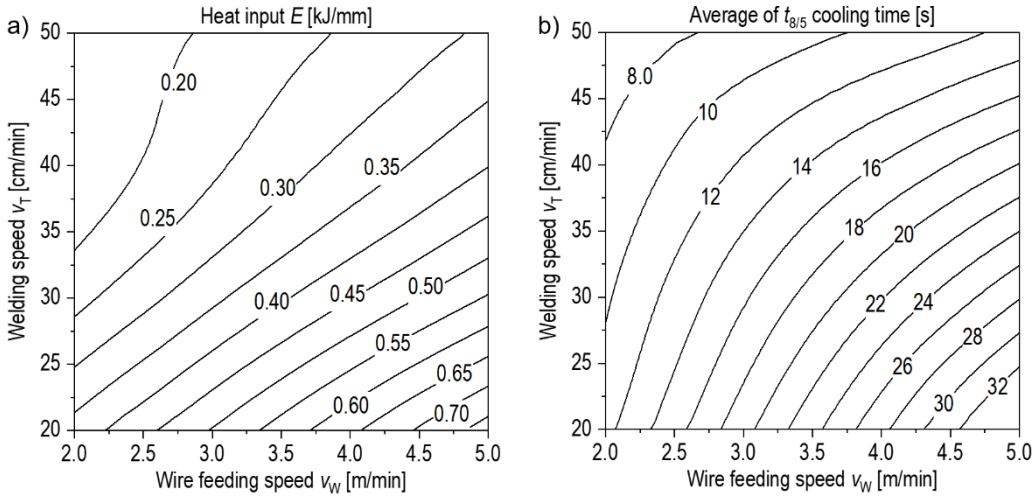

Figure 7. Heat input E (a) and average of $t_{8/5}$ cooling time (b) as a function of wire feeding and welding speed in the investigated parameter range (contour plots of the regression models).

Moreover, figure 7a reveals that at higher welding speeds and also at higher wire feed rates, the layer width and the energy per unit length decouple to a certain extent. The influence of the welding speed

remains more or less the same even at higher values for the energy per unit length but is less pronounced on the layer width. This is due to the direct relationship between welding speed and heat input. A lower heat input ultimately results in reduced dilatation of the layers and an earlier solidification. A similar effect can be seen at higher wire feeding speeds. Here the influence of the welding speed on the heat input is even somewhat greater, but at the same time the influence on the layer width decreases somewhat in comparison, especially for high welding speeds. When welding high-strength fine-grained structural steels, the special microstructure requires a cooling rate to be kept within a tight interval ($t_{8/5}$ cooling time range). The cooling time and thus the heat control during welding significantly affects the resulting mechanical-technological properties of the generated component. During WAAM, similar to multi-layer welding, each layer undergoes a complex heat treatment consisting of multiple cyclic heating and cooling.

Figure 7b shows the contour plot of the last measurable $t_{8/5}$ cooling times (i.e. with peak temperature >800 °C) of the 5th layer as function of welding speed and wire feed rate. In the derived regression model of the resulting cooling times, the wire feed rate and the interaction of wire feed rate and welding speed are highly significant. The model quality is high with R^2=0.953. By comparison with the determined average $t_{8/5}$ cooling times, a correlation with the heat input reveals. It is apparent that the influence of the wire feed rate on cooling time decreases as the welding speed increases towards lower values for the cooling time. This is mainly due to the relatively large influence on the layer width in this area. As a result, at high welding speed and with increasing wire feed rate, the layer width increases at a higher rate than the heat input. The increased layer width results in a better adhesion to the layers below and an enhanced heat transfer, which results in a faster heat dissipation from the welded layer.

3.3. Residual stress analysis

The residual stress analysis by means of XRD at the top layer of the two WAAM test specimens is presented in figure 8. Remarkably, the residual stresses in the transverse direction of the welded layers or walls for both specimens are significantly higher than those in the direction longitudinal to the weld, despite the high shrinkage restraint in the longitudinal direction caused by the underlying layers. Yet, it reveals that an increasing restraint in transverse direction in near the corner of the hollow cuboids causes for both specimen bodies the highest tensile residual stresses of approx. 350 MPa at these locations. The maximal longitudinal residual stresses are present in a certain distance of the corners.

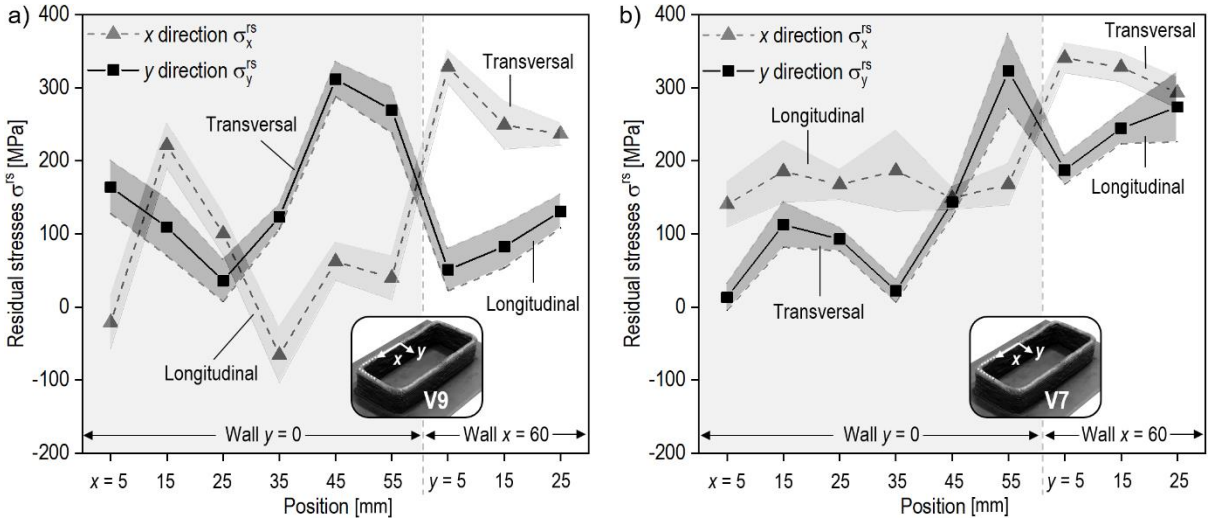

Figure 8. Residual stress distributions $\sigma^{rs}(x,y)$ and error range at the top layer of the WAAM test specimens: a) V9 (E=0.18 kJ/mm, $t_{8/5}$=9.2 s) and b) V7 (E=0.43 kJ/mm, $t_{8/5}$=20.2 s).

By comparison of both components, longitudinal tensile residual stresses reveal to be considerably higher in case of increased heat input for both side walls of the hollow cuboid, as shown for test V7 in figure 8b. Figure 9 reveals in particular for the short side walls a difference of approx. 150 MPa.

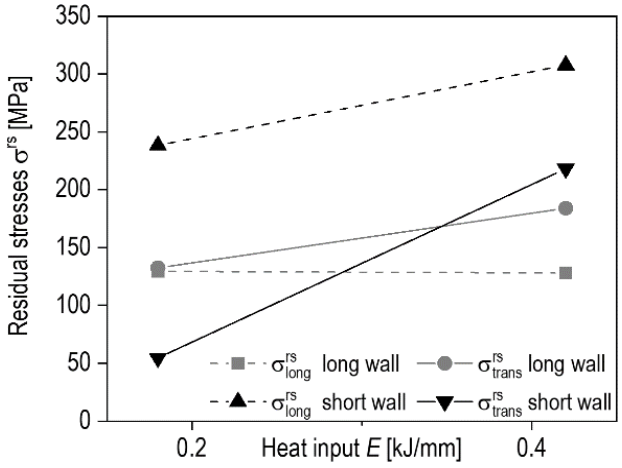

Figure 9. Effect diagram of averaged transversal and longitudinal residual stress levels at the top layer of the short and long side walls of the hollow cuboids depending on the applied heat input *E* during welding.

The higher heat input as well leads to higher transverse residual stresses, especially at the short side wall. According to the common concepts of residual stress evolution in steels with undergoing phase transformation this is primarily due to the higher volume of heated material combined with an increased restrained shrinkage initiating higher tensile stresses while cooling and, furthermore, due to the different microstructure developing at higher cooling times [17, 18]. It is assumed that shorter cooling times lead to a microstructure with a higher share of bainite and martensite instead of a ferritic microstructure. Thereby a higher volume expansion occurs during the phase transformation, the hindrance of which leads to the formation of compressive stresses or to compensation of arising tensile stresses [19, 21]. However, as figure 8a reveals for test V9, the gradients of the longitudinal stresses are higher at the long side wall of the specimen welded with lower heat input, which is due to local effects in connection with the phase transformation. The averages for the residual stresses longitudinal and transverse to the weld are shown in figure 9 in an effect diagram for the short and the long side walls dependent on the applied heat input during welding. It is noticeable that the mean longitudinal residual stresses over the long side wall are hardly affected depending on the heat input, which is assumed to be due to the relatively thin substrate plate of 4 mm and the resulting deformation during welding. The greatest effect can be observed with the short side walls which are supposed to be effectively restrained by the long side walls. Longitudinal and transversal residual stresses increase due to the higher heat input.

4. Conclusions

In the present study, the influences welding speed and wire feed rate on the layer geometry, cooling time and residual stresses of additively manufactured components made of high-strength fine-grained structural steels were investigated.

(1) Welding consumables specially developed for WAAM have a modified flow behavior, and in contrast to conventional filler metals, lead to an increased layer height with reduced widths. The cross sections of the additively welded walls show a suitable microstructure and that the special WAAM welding filler material AM 80 solidifies fine-grained.

(2) An enlarged parameter range for the application of the filler material serves facilitating additive production steps, especially in the case of complex geometries. It can be assumed that this ultimately has a positive effect on the mechanical-technological properties, which is subject to further investigations in the research project.

(3) By deriving regression models, effects and interactions of the welding parameters on the target quantities were found, interpretations as operating characteristics of the WAAM system used are achievable. With these characteristic curves, suitable starting points for the calibration of the generation process can be identified and slicer programs can be optimized for the WAAM process.

(4) The relationships shown also clarify the fundamental influence of welding and wire feeding speed on the cooling time and the residual stress build-up, which is superimposed by cooling time dependent effects, e.g. phase transformation.

(5) The residual stresses are depending on the heat input or cooling time, respectively. For higher heat input, an increase in residual stress level were found, especially in transverse direction to the weld. The highest increase was found in the short side wall. The low effect in longitudinal direction of the long side wall is assumed to be due to low restraint of the applied substrate plate.

These findings and correlations form the basis for the next steps of the planned investigations, e.g. with focus on the influences of component design and build-up strategy on the residual stress evolution. Additionally, the restraint during welding of the component will be significantly increased due to application of heavy and rigid substrate plates for further experiments. Furthermore, the effect of the heat control on the microstructure formation has to be clarified in detail, especially considering a homogeneous distribution with respect to the resulting component properties.

Acknowledgments
The studies were funded by the AiF-project project IGF-Nr. 21162 BG/FOSTA P1380. Sincere thanks are given for this support and to the representing companies actively involved in the project board.

References

[1] Raoul J 2005 *Use and Application of High-Performance Steels for Steel Structures* ed Guenther H-P (Zürich: IABSE) p 152
[2] Hulka K, Kern A and Schriever U 2005 *Materials Science Forum* **500-501** 519-526
[3] German Federal Ministry for the Environment (BMU) 2019 *Climate Action in Figures*
[4] Plangger J, Schabhüttl P, Vuherer T and Enzinger N 2019 *Metals* **9**
[5] Frazier W E 2014 *Journal of Materials Engineering and Performance* **23** 1917-1928
[6] voestalpine Böhler Welding Group GmbH 2018 *The Future of Productivity: Wire Arc Additive Manufacturing (WAAM)* p 12
[7] Ding D, Pan Z, Cuiuri D and Li H 2015 *International Journal of Advanced Manufacturing Technology* **81** 465-481
[8] Rodrigues T A, Duarte V, Miranda R M, Santos T G and Oliveira J P 2019 *Materials (Basel)* **12**
[9] Xizhang C, Su C, Wang Y, Siddiquee A N, Sergey K, Jayalakshmi S and Singh R A 2019 *Journal of Surface Investigation: X-ray, Synchrotron and Neutron Techniques* **12** 1278-1284
[10] Graf M, Hälsig A, Höfer K, Awiszus B and Mayr P 2018 *Metals* **8** 1009
[11] Ogino Y, Asai S and Hirata Y 2018 *Welding in the World* **62** 393-401
[12] Schroepfer D, Kromm A, Schaupp T and Kannengiesser T 2018 *Welding in the World* **63** 647-661
[13] European Standard EN 1011-2 2001 *Welding - Recommendation for welding of metallic materials - Part 2: Arc welding of ferritic steels*
[14] Technical guideline SEW 088 2017 *Weldable non-alloy and low-alloy steels Recommendations for processing, in particular for fusion welding* (Düsseldorf: Stahleisen GmbH) p 52
[15] European Standard EN 1993 2010 *Eurocode 3: Design of steel structures*
[16] Hönnige J, Seow C E, Ganguly S, Xu X, Cabeza S, Coules H and Williams S 2020 *Materials Science and Engineering: A* [https://doi.org/10.1016/j.msea.2020.140368]

[17] Wohlfahrt H 1987 *Advances in Surface Treatments Vol. 4 - International Guidebook on Residual Stresses*, p 40-58
[18] Schroepfer D, Kromm A and Kannengiesser T 2018 *Welding in the World* **63** 43-51
[19] Schroepfer D, Kromm A and Kannengiesser T 2015 *Welding in the World* **59** 455-464
[20] Fuchs C, Baier D, Semm T and Zaeh M F 2020 *Production Engineering* **14** 629-637
[21] Bhadeshia H K D H 2004 *Materials Science and Engineering A* **378** 34-39